



Promotion of the Rapid Growth in *Haematococcus pluvialis* Under 0.16% CO₂ Condition Revealed by Transcriptome and Metabolomic Analysis

Xin Ye¹ · Jiani Chen¹ · Chaoyang Hu¹ · Nianjun Xu¹ · Xue Sun¹

Received: 14 May 2019 / Accepted: 7 November 2019 / Published online: 25 November 2019
© Springer Science+Business Media, LLC, part of Springer Nature 2019

Abstract

The unicellular green alga *Haematococcus pluvialis* is considered the optimal natural source of astaxanthin, a strong antioxidant in nature. In the present study, transcriptome and metabolic profiling of *H. pluvialis* under 0.16% and 0.04% CO₂ levels were performed to explore the underlying mechanism by which CO₂ affects growth at the vegetative stage of this alga. Approximately 1665 differentially expressed unigenes were screened in response to different CO₂ conditions by transcriptome analysis. The genes related to photosynthesis, the tricarboxylic acid (TCA) cycle, glycolysis, pentose phosphate pathway, and nitrogen metabolism, were mostly up-regulated by 0.16% CO₂. A total of 36 differential metabolites were identified in metabolic profiling, of them, citric acid and ribose were accumulated; however, 12 common amino acids and stress-resistant related substrates such as ornithine and putrescine were decreased at 0.16% CO₂ level. Combining the results of the algal growth, the elevated CO₂ promoted photosynthesis, and carbon utilization including TCA cycle and glycolysis, together with the stimulated nitrogen metabolism, protein synthesis, and energy metabolism, which resulted in rapid growth of *H. pluvialis*.

Keywords *Haematococcus pluvialis* · Rapid growth · CO₂ concentration · Transcriptome · Metabolomic profiling

Introduction

Astaxanthin is a kind of carotenoid compound with strong antioxidant activity, which is used in aquaculture, various pharmaceuticals, and cosmetics (Wayama et al. 2013). The unicellular green alga *Haematococcus pluvialis*, currently regarded as *Haematococcus lacustris*, can accumulate high levels of astaxanthin (Boussiba 2000). The life cycle of *H. pluvialis* can be divided into a green vegetative stage and a red cyst (aplanospore) stage. In the green stage, *H. pluvialis* grows under suitable conditions, while in the red stage, thick-walled spores form and large amounts of astaxanthin accumulate in unfavorable environments (Hagen et al. 2002).

Due to the great commercial value, scientific researches and manufactures are interested in the growth and astaxanthin accumulation of *H. pluvialis*. A two-step method with promoting algal growth firstly and then inducing astaxanthin accumulation is usually used in this algal aquaculture industry (Christian et al. 2018). In addition, culture conditions such as light, nutrients, and temperature are widely studied in order to achieve the optimal growth rate and astaxanthin production in *H. pluvialis* (Imamoglu et al. 2007; Wan et al. 2014).

In recent years, increasing numbers of high-throughput sequencing and metabolomics studies have been applied to *H. pluvialis*. The mechanism of astaxanthin accumulation induction by phytohormones in *H. pluvialis* has been analyzed using transcriptome sequencing (Gao et al. 2015). A total of 2245 and 171 differentially expressed genes (DEGs) have been identified in *H. pluvialis* in response to blue-light and red-light irradiation, respectively (Lee et al. 2018). Gas chromatography–mass spectrometry (GC–MS) analysis revealed that α -ketoglutaric acid, glutamic acid, and ribulose-5-phosphonate were associated with the Fe²⁺ and high light conditions (Su et al. 2014). Eighty-one metabolites were identified and quantified by GC–MS, and some

Electronic supplementary material The online version of this article (<https://doi.org/10.1007/s00344-019-10055-6>) contains supplementary material, which is available to authorized users.

✉ Xue Sun
sunxue@nbu.edu.cn

¹ Key Laboratory of Marine Biotechnology of Zhejiang Province, School of Marine Sciences, Ningbo University, Ningbo 315211, China

cytoprotective metabolites were increased during the astaxanthin accumulation process in *H. pluvialis* (Lv et al. 2016).

Comparatively, more attention is paid to the accumulation of astaxanthin other than the vegetative growth of the alga. In the present study, the growth, transcriptome and metabolomic profiles of *H. pluvialis* are studied response to two CO₂ levels. The aim of this study is to elucidate the underlying mechanisms of CO₂ on *H. pluvialis* and to identify the key metabolites that influence the rapid growth of this species.

Materials and Methods

Haematococcus pluvialis Cultivation

Haematococcus pluvialis strain 489 was obtained from the Key Laboratory of Marine Biotechnology of Zhejiang Province in Ningbo University. The axenic algae were cultured under conditions of 25 ± 1 °C, and 40 μmol/ (m² s) light intensity with a 12 h: 12 h light: dark cycle. *H. pluvialis* in the logarithmic growth phase were inoculated into fresh NMB3[#] medium (Wang et al. 2014). The algae were cultivated under two CO₂ levels: one was cultured under a normal air (0.04% CO₂, the control), while the other was cultured under a fourfold higher air CO₂ concentration (0.16% CO₂).

Growth and Chemical Composition Measurement

H. pluvialis was transferred to 150 mL fresh media in a 250 mL flask with an inoculation ratio of approximately 4.50 × 10⁴ cells/mL, and OD₆₈₀ was measured daily until 8 days. The algal cell density was calculated based on the linear equation of OD₆₈₀ and cell density.

The protein content of this alga was quantified by bicinchoninic acid (BCA) assay (Walker 1994). The polysaccharide and lipid contents were determined by anthrone and vanillin methods using colorimetry, respectively (Morris 1948; Kushiro et al. 1972). The chlorophyll was extracted by acetone and measured according to the method described by Mackinney (1941). All assays were performed in triplicate, and data were shown as the means ± SD (*n* = 3).

Total RNA Extraction, cDNA Library Construction, and RNA-seq

On the mid-log phase (day 6), 30 mL algal samples were harvested by centrifugation at 7000 g for 5 min from each flask, respectively, and then total RNA was extracted using TRIzol reagent (Invitrogen, CA, USA). Each group included three replicates. The RNA integrity was determined by agarose gel electrophoresis, and the RNA concentration and

purity were assayed with a NanoDrop 1000 Spectrophotometer (Thermo Scientific, MA, USA).

Total RNA that met the quality standards was used to construct a cDNA library through a series of processes including RNA purification, mRNA isolation and fragmentation, double-stranded cDNA synthesis, adaptor ligation, and enrichment. The constructed cDNA library was tested with an Agilent 2100 Bioanalyzer. Then, an Illumina HiSeq 4000 platform was used for sequencing.

Data Assembly and Unigene Annotation

The raw reads obtained by sequencing were subjected to data processing. After filtering out low-quality sequences, adaptor sequences, and fuzzy data, clean data were de novo assembled using Trinity v2.0.6, and then TGICL v2.0.6 was used to cluster the transcripts into unigenes.

The Basic Local Alignment Search Tool (BLAST) v2.2.23 was used to align and annotate the unigenes with the non-redundant nucleotide sequences (NT), non-redundant protein sequences (NR), Cluster of Orthologous Groups of proteins (COG), Kyoto Encyclopedia of Genes and Genomes (KEGG), and SwissProt databases. Gene Ontology (GO) annotation was performed after combining the Blast2GO v2.5.0 results with the NR annotations (Conesa et al. 2005), and InterProScan5 v5.11–51.0 was used to perform InterPro annotation (Quevillon et al. 2005).

Annotation, GO and KEGG Enrichment Analysis of DEGs

The clean reads were mapped to unigenes using Bowtie2 v2.2.5 (Langmead and Salzberg 2012), and the gene expression levels were calculated with RSEM v1.2.12 (Li and Dewey 2011). The DEGs were detected with NOIseq based on the noisy distribution model with criteria of a log₂ (fold change) ≥ 1 and probability > 0.8 (Tarazona et al. 2011).

GO and KEGG functional enrichment analysis of the DEGs was performed using the phyper function in R software. The false discovery rate (FDR) was calculated for each *p* value, and terms with an FDR ≤ 0.01 were defined as significantly enriched.

Validation by Quantitative Real-Time PCR (qPCR)

From these DEGs, 8 were selected for qPCR validation. The primers were designed with Primer Premier 5.0 software (Supplementary Table S1). The sample treatments and total RNA extraction were the same as those used in preparation for transcriptome sequencing. β-actin was used as the internal standard (Huang et al. 2006). The results were presented as the means of three replicates. The relative expression of the genes was calculated with the 2^{-ΔΔCT} method (Livak and Schmittgen

2001), and a fold change > 2 or < 0.5 was considered a significant difference (Chang et al. 2014).

Extraction and Detection of Metabolites

Algal samples were collected on day 6 for extracting the metabolites. Approximately 60 ± 1 mg sample were extracted using methanol: H_2O (3:1, v/v) and adonitol, and then were ground and treated by ultrasonication in triplicate. After centrifugation by 14,000 g for 15 min at 4 °C, the supernatant was dried by vacuum concentrator. Finally, after incubation at 80 °C for 30 min in methoxyaminatio hydrochloride reagent and 70 °C for 1.5 h in BSTFA containing 1% TMCS (v/v), the samples were ready for detection of the metabolites.

Agilent DB-5MS capillary column (30 m \times 250 μ m \times 0.25 μ m, USA) were used in the GC-TOF-MS (Agilent 7890). The parameters were listed as the following: Front inlet (splitless) mode, 1 mL/min column flow, oven temperature ramp of 50 °C hold on 1 min, raised to 310 °C at a rate of 10 °C/min, and hold on 8 min; 280 °C front injection and transfer line temperature, and 250 °C ion source temperature, with a mass range of m/z:50–500.

Data Precession and Metabolites Analysis

The raw data were processed by filtration of noise and single peak, simulation of the missing value, and normalization. The SIMCA14.1 software (MKS Data Analytics Solutions, Umea, Sweden) was used to the principal component analysis (PCA) and orthogonal projections to latent structures-discriminant analysis (OPLS-DA) (Tsubawa et al. 2011; Abdi and Williams 2010; Wiklund et al. 2008). Multivariate statistical analysis method was used with the criteria of p value of student's t -test < 0.05 , and the Variable Importance in the Projection (VIP) of the first principal component in OPLS-DA model > 1 .

Annotation and Pathway Analysis of Metabolites

KEGG annotation was performed against the KEGG database (Kanehisa et al. 2015). The pathway was further mapped to the databases of KEGG and PubChem, and then screened to the pathways by the enrichment and topology analysis. Complete linkage method was used to cluster differential metabolites based on the euclidean distance matrix calculated by the quantitative value of the differential metabolites.

Results

Comparison of the Algal Growth and Chemical Parameters

The growth of *H. pluvialis* was affected significantly by the CO_2 level (Fig. 1). In 0.16% CO_2 group, the cell density increased rapidly, and it reached 2.36-fold of that in the control group on day 8 ($p < 0.05$). However, a slow growth rate was observed at 0.04% CO_2 with a 3.52-fold increment on day 8 relative to the initial inoculation density, which was slower than the 8.40-fold increase in 0.16% CO_2 group.

The soluble protein in 0.16% CO_2 group increased 1.64-fold higher levels than that in the control group. On the contrary, other chemical parameters such as polysaccharide, total lipid, and chlorophyll were all decreased by the elevated CO_2 treatment ($p < 0.05$) (Supplementary Table S2).

Data Assembly and Unigene Annotation

A total of 40.09 Gb of clean bases were obtained from 6 groups, with the bases for each group ranging from 6.63 to 6.74 Gb. The clean reads percentages ranged from 72.66 to 78.23%, with a Q20 of 97.0%. After assembly, a total of 73,549 unigenes were obtained with 82.82 Mb total length; the average length and N50 of all the unigenes were 1126 bp and 1878 bp, respectively (Table 1). The GC

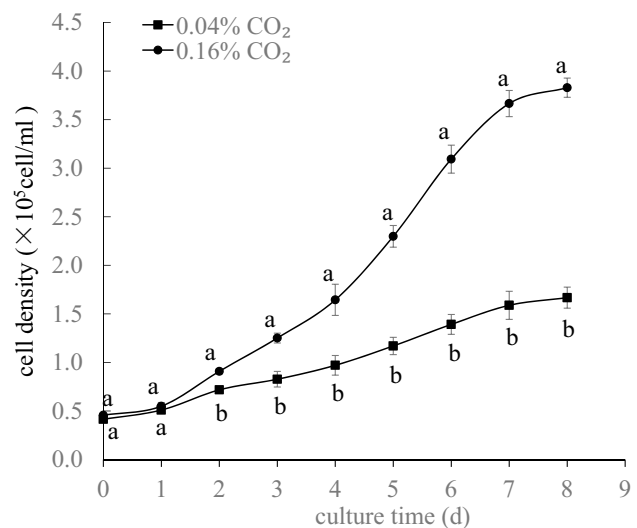


Fig. 1 The growth curves of *H. pluvialis* under two CO_2 concentrations. The error bars represent SD, as described in “Materials and methods” section; the different letters represent significant differences ($p < 0.05$)

Table 1 Statistics for the assembled unigenes in RNA-seq data of *H. pluvialis*

Sample	Total number	Total length (Mb)	Mean length (bp)	N50 (bp)	GC (%)
0.16% CO ₂ -1	48,101	40.78	847	1352	59.84
0.16% CO ₂ -2	48,770	42.50	871	1394	60.14
0.16% CO ₂ -3	46,085	39.90	865	1380	60.02
0.04% CO ₂ -1	45,703	42.07	920	1447	60.85
0.04% CO ₂ -2	48,490	44.20	911	1461	60.77
0.04% CO ₂ -3	45,575	41.90	919	1451	60.83
All-unigenes	73,549	82.82	1126	1878	60.22

Table 2 Statistics for the annotated unigenes in the databases in RNA-seq data of *H. pluvialis*

Database	Number of annotated unigenes	Percentage of annotated unigenes (%)
NR	40,443	54.99
NT	23,303	31.68
SwissProt	27,843	37.86
KEGG	31,833	43.30
COG	21,871	29.74
InterPro	20,785	28.26
GO	12,258	16.67
Total	45,291	61.58

content of the *H. pluvialis* sequences was approximately 60.22%. Most unigenes (12,829) were short, with lengths between 300–400 bp, while 1071 unigenes had lengths equal to or greater than 3000 bp.

Of the total of 73,549 unigenes, 61.58% were annotated in the 7 databases (Table 2). The NR database had the greatest number of annotated unigenes of 40,433; these unigenes accounted for 54.99% of all the unigenes. A total of 43.30% of the unigenes were annotated in the KEGG database, while 37.86% were annotated in the SwissProt database. The GO database had the least annotated unigenes at 16.67%.

The numbers of unigenes annotated in the NR, COG, KEGG, SwissProt, and InterPro databases are shown in a Venn diagram (Fig. 2); a total of 11,885 unigenes (16.16%) were shared among the 5 databases.

Results of DEGs Analysis

In this study, 1665 DEGs were screened, among which 772 were up-regulated and 893 were down-regulated by elevated CO₂ concentration. A portion of the annotated unigenes are listed in the following.

Photosynthesis- and chloroplast-related DEGs: Among the DEGs in *H. pluvialis* related to photosynthesis and chloroplasts, almost all were promoted by 0.16% CO₂ concentration (Table 3). Components of photosystem I and

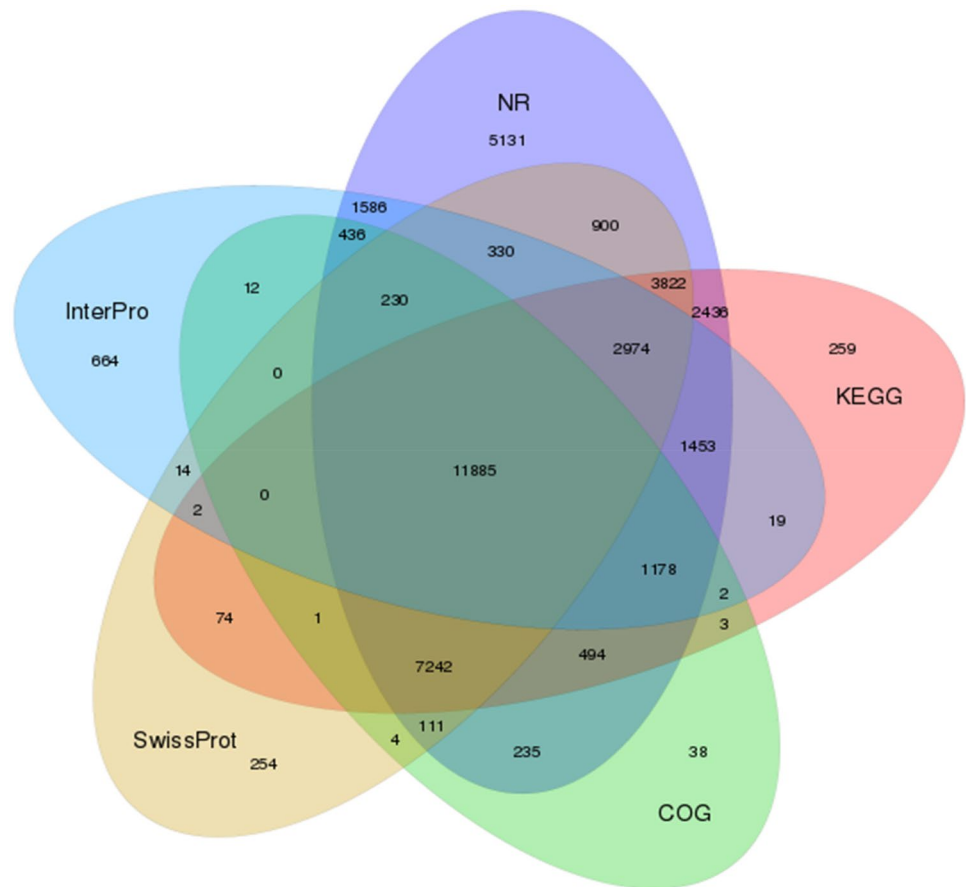
photosystem II, e.g., P700 apoprotein A2 (Unigene22221_All), subunit IX of photosystem I (Unigene22221_All), D1 reaction center protein (CL6274.Contig2_All), CP43 (Unigene807_All), psbB (CL3570.Contig3_All), were all up-regulated; moreover, CF0 subunit I and subunit IV of ATP synthase (Unigene16856_All, CL8558.Contig4_All) and apocytochrome f of cytochrome b6/f complex (Unigene8874_All) were also induced in 0.16% CO₂ group. Light-harvesting proteins are involved in capturing light energy and in regulating light energy distribution, absorption and transmission. Seven DEGs relevant to these antenna proteins, including light-harvesting chlorophyll a/b protein 3 (Unigene3840_All, Unigene2697_All), chlorophyll a/b binding protein Lhca6 (Unigene2557_All), light-harvesting protein of photosystem II (Unigene4943_All), were all up-regulated by 0.16%CO₂.

In addition, all ribosomal proteins in the chloroplast, including the small ribosomal protein subunits S3, S4, S9 (2 DEGs), S11, and S12 and the large ribosomal protein subunits L5, L14, L23 (2 DEGs), and L32 (2 DEGs), were all up-regulated in 0.16% CO₂ group. The various cell division proteins (5 DEGs) were all induced by 0.16% CO₂.

The expression levels of the ChlB (Unigene11063_All) and ChlN (CL2898.Contig2_All, CL2898.Contig3_All) subunits of light-independent protochlorophyllide reductase, which are responsible for chlorophyll synthesis in the dark, were up-regulated. Protoporphyrin IX magnesium chelatase (ISS) is a key enzyme in chlorophyll synthesis, and one ISS gene (Unigene18576_All) was down-regulated, which might be related to the decreased chlorophyll content in 0.16% CO₂ group.

Carbohydrate metabolism-related DEGs (Fig. 3 and Table 4): In the glycolysis pathway, one gene encoding phosphoglycerate kinase (PGK; CL6807.Contig1_All) and two other glycolysis-related enzymes, glucose-6-phosphate isomerase (Unigene14387_All) and glyceraldehyde 3-phosphate dehydrogenase (GAPDH, Unigene22448_All), were up-regulated by 0.16% CO₂. Two pyruvate kinase-encoding genes (CL10817.Contig1_All, Unigene3795_All) were up-regulated 16.91-fold and 6.73-fold, respectively, while two other pyruvate kinases (Unigene19963_All,

Fig. 2 Venn diagram of the annotated unigenes of *H. pluvialis*. The different ellipses represent different databases; the numbers represent the unique or the common unigenes annotated in the databases



Unigene31645_All) were down-regulated to 0.21 times and 0.19 times of those in 0.04% CO₂ group, respectively.

In TCA cycle, three genes encoding aconitase (aconitate hydratase; CL2951.Contig1_All, CL2951.Contig2_All, CL2951.Contig3_All) were up-regulated by 0.16% CO₂ concentration. In addition, the expression of two NAD-dependent isocitrate dehydrogenase (NAD-IDH) genes (CL8074.Contig1_All, CL8074.Contig2_All) was increased, while that of another two NADP-dependent isocitrate dehydrogenase (NADP-IDH) genes (CL3305.Contig2_All, CL3305.contig3_All) were decreased. The NAD-IDH is involved in TCA cycle in eukaryotic cells, and two NADP-IDH is not used for energy supply. Two genes encoding malate dehydrogenase showed the same pattern as that of isocitrate dehydrogenase, with one gene (CL7051.Contig7_All) up-regulated and another (CL9961.Contig2_All) down-regulated. However, the down-regulated malate dehydrogenase gene was not annotated in the KEGG database, so it was not included in the metabolic pathway analysis.

Other carbohydrate metabolism-related genes were also identified. The enzyme 6-phosphogluconate dehydrogenase (decarboxylating) is responsible for oxidative decarboxylation of 6-phosphogluconate to ribulose 5-phosphate and CO₂. One 6-phosphogluconate dehydrogenase

(decarboxylating) gene (CL2177.Contig2_All) and three glucose-6-phosphate dehydrogenase (G6PDH) genes (CL8925.Contig2_All, CL8925.Contig3_All, CL8925.Contig4_All) were all induced by elevated CO₂ concentration. The two enzymes participate in pentose phosphate pathway, and the pathway is parallel to the glycolysis pathway.

Formate C-acetyltransferase (pyruvate formate lyase) contributes to the reversible conversion of pyruvate and coenzyme A into formate and acetyl-CoA. Two pyruvate formate lyase (CL2733.Contig2_All, CL2733.Contig3_All), and one pyruvate formate lyase activating enzyme (CL140.Contig2_All) were increased. Pyruvate decarboxylase catalyzes the decarboxylation of pyruvic acid to acetaldehyde and carbon dioxide. The expression of two pyruvate decarboxylase genes (CL2766.Contig1_All, CL2766.Contig3_All) was up-regulated. However, the expression profiles of sulfated surface glycoprotein 185 (CL9309.Contig2_All, Unigene20978_All, CL5904.Contig3_AI), cellulose synthase (Unigene23043_All), cellulase (CL7979.Contig1_All), starch synthase (CL7668.Contig1_All), and glycosyl hydrolase family 32 (CL7447.Contig1_All) were all down-regulated by 0.16% CO₂.

Nitrogen metabolism-related DEGs: In 0.16% CO₂ group of *H. pluvialis*, the expression levels of nitrate

Table 3 List of photosynthesis- and chloroplast-related differentially expressed genes of *H. pluvialis* under two CO₂ concentrations

Gene ID	Log ₂ FC	Gene annotation
CL6274.Contig2_All	4.01	D1 reaction center protein of photosystem II (chloroplast)
Unigene807_All	3.06	CP43 chlorophyll apoprotein of photosystem II (chloroplast)
CL10087.Contig4_All	6.54	10 kDa photosystem II polypeptide
Unigene22221_All	2.99	P700 apoprotein A2 of photosystem I (chloroplast)
CL5212.Contig1_All	3.58	Subunit IX of photosystem I (chloroplast)
CL3570.Contig3_All	2.00	PsbB
Unigene21869_All	3.63	J protein of photosystem II (chloroplast)
Unigene13073_All	4.80	M protein of photosystem II (chloroplast)
Unigene16856_All	3.44	CF0 subunit I of ATP synthase (chloroplast)
CL8558.Contig4_All	1.97	CF0 subunit IV of ATP synthase (chloroplast)
Unigene8874_All	3.40	apocytochrome f of cytochrome b6/f complex (chloroplast)
Unigene3840_All	2.15	Major light-harvesting chlorophyll a/b protein 3
Unigene2697_All	2.02	Major light-harvesting chlorophyll a/b protein 3
Unigene2557_All	1.85	Light-harvesting chlorophyll a/b binding protein Lhca6
Unigene4943_All	2.20	Light-harvesting protein of photosystem II
CL9882.Contig2_All	2.36	Major light-harvesting complex II protein m9
Unigene2577_All	2.84	Chlorophyll a-b binding protein of LHCII type I,
Unigene5335_All	2.13	Chlorophyll a-b binding protein of LHCII
Unigene9150_All	2.96	Ribosomal protein S3 (chloroplast)
Unigene15167_All	2.38	Ribosomal protein S4 (chloroplast)
Unigene8961_All	2.18	Ribosomal protein S9 (chloroplast)
Unigene8866_All	2.69	Ribosomal protein S9 (chloroplast)
Unigene9193_All	4.29	Ribosomal protein S11 (chloroplast)
Unigene8922_All	3.29	Ribosomal protein S12 (chloroplast)
CL3789.Contig1_All	4.14	Ribosomal protein L5 (chloroplast)
Unigene12007_All	8.89	Ribosomal protein L14 (chloroplast)
Unigene8899_All	1.99	Ribosomal protein L23 (chloroplast)
Unigene8888_All	3.12	Ribosomal protein L23 (chloroplast)
Unigene14567_All	3.10	Ribosomal protein L32 (chloroplast)
Unigene14568_All	3.54	Ribosomal protein L32 (chloroplast)
CL10656.Contig3_All	2.10	Cell division protein (chloroplast)
CL10656.Contig4_All	1.92	Cell division protein (chloroplast)
Unigene8940_All	2.54	Cell division protein (chloroplast)
Unigene8950_All	1.97	Cell division protein (chloroplast)
Unigene20520_All	4.40	Cell division protein (chloroplast)
Unigene11063_All	4.09	ChlB subunit of protochlorophyllide reductase (chloroplast)
CL2898.Contig2_All	2.13	ChlN subunit of protochlorophyllide reductase (chloroplast)
CL2898.Contig3_All	2.03	ChlN subunit of protochlorophyllide reductase (chloroplast)
CL9900.Contig1_All	7.28	Translational elongation factor Tu (chloroplast)
CL8906.Contig2_All	7.84	CPD photolyase class II
CL8906.Contig3_All	3.80	CPD photolyase class II
CL2184.Contig1_All	3.79	Chlorophyll a oxygenase
Unigene7639_All	4.23	Envelope membrane protein (chloroplast)
Unigene18634_All	− 5.29	Heme attachment to plastid cytochrome c (chloroplast)
Unigene18576_All	− 2.50	Protoporphyrin IX magnesium chelatase (ISS)
Unigene2897_All	− 1.86	Rhythm of chloroplast 75
CL3919.Contig3_All	− 2.22	Phycocyanobilin:ferredoxin oxidoreductase

FC, fold changes of the gene expression (group 0.04% CO₂ vs. 0.16% CO₂)

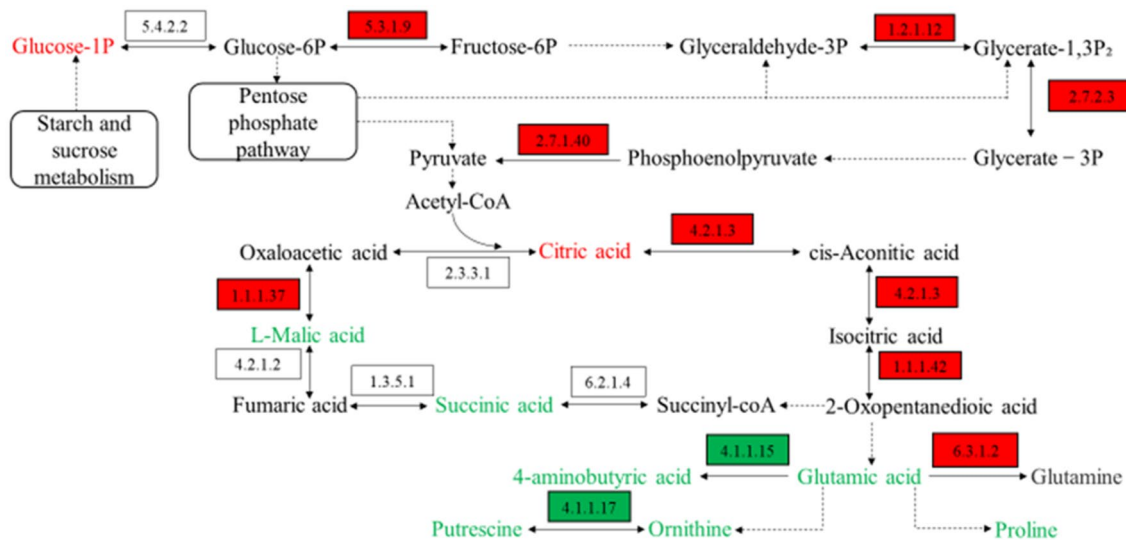


Fig. 3 Effects of 0.16% CO₂ on the genes and metabolites in glyco-metabolism-related pathway of *H. pluvialis*. The up-regulated genes or metabolites are noted as red; the down-regulated genes or metabolites are noted as green. The “phosphate” in the metabolites is abbreviated as “P”. The enzyme numbers and their corresponding names are listed: 5.3.1.9, glucose-6P isomerase; 1.2.1.12, glyceraldehyde 3P

dehydrogenase; 2.7.2.3, phosphoglycerate kinase; 2.7.1.40, pyruvate kinase; 4.2.1.3, mitochondrial aconitate hydratase; 1.1.1.42, isocitrate dehydrogenase; 1.1.1.37, malate dehydrogenase; 6.3.1.2, glutamine synthetase; 4.1.1.15, glutamate decarboxylase; 4.1.1.17, ornithine decarboxylase

reductase (CL3917.Contig3_All, CL3917.Contig4_All), assimilatory nitrite reductase (CL1166.Contig1_All), and nitrate transporter (7 DEGs) were all up-regulated (Supplementary Table S3). Two ammonium transporters (Unigene16043_All, Unigene1816_All) were increased, and one ammonium transporter (Unigene2449_All) was decreased in 0.16% CO₂ group. Although two cationic amino acid transporters (CL7923.Contig1_All, CL7923.Contig5_All) were induced, two amino acid transporters (CL9492.Contig1_All, CL9492.Contig3_All) were depressed. Two glutamine synthetase genes (CL599.Contig1_All, CL599.Contig2_All) were up-regulated, while the expression tendencies of two glutamate decarboxylases (CL6019.Contig7_All, Unigene26503_All) were opposite.

Lipid metabolism-related DEGs: In contrast to the large number of carbohydrate metabolism-related unigenes, a small number of lipid metabolism-related unigenes were found to be differentially expressed in response to different CO₂ levels (Supplementary Table S3). Among them, genes encoding acetyl-CoA synthetase (CL5434.Contig1_All), alcohol dehydrogenase (CL2043.Contig3_All and Unigene17063_All), and geraniol dehydrogenase (CL2043.Contig2_All) were up-regulated in response to 0.16% CO₂ level. Other lipid related unigenes, such as fatty acyl-CoA reductase 2, glycerol-3-phosphate acyltransferase, triacylglycerol lipase, and ethanolamine phosphotransferase, were all down-regulated under 0.16% CO₂ concentration. One diacylglycerol kinase (CL525.Contig7_All) was

induced, while two other diacylglycerol kinases (Unigene18613_All, Unigene10034_All) were inhibited.

Astaxanthin synthesis-related DEGs: Several astaxanthin synthesis-related genes were found to be differentially expressed in response to the different CO₂ concentrations (Supplementary Table S3). Among them beta-carotene ketolase (bkt1) genes were the most (5 DEGs: CL5434.Contig1_All, CL3712.Contig3_All, CL6433.Contig4_All, CL6789.Contig2_All, CL964.Contig6_All). Besides the five beta-carotene ketolases, one carotenoid hydroxylase (Unigene31321_All), one phytoene synthase (Unigene28954_All), and one beta-carotene C-4 oxygenase (Unigene1990_All) were up-regulated; in contrast, one lycopene beta cyclase (CL9386.Contig1_All), and one zeta-carotene desaturase (Unigene4251_All) were down-regulated under 0.16% CO₂ concentration. Among the down-regulated genes, lycopene beta cyclase and zeta-carotene desaturase are directly responsible for beta-carotene synthesis.

Heat shock protein-related DEGs: In 0.16% CO₂ group, all heat shock protein-related genes except one, Hsp70D (Unigene1107_All), were down-regulated, including heat shock proteins 70C, 70E, 90, 90B, and 22A; Hsp70-Hsp90 organizing protein; and other molecular chaperones (Supplementary Table S3).

Other DEGs: a large number of other unigenes was affected by different CO₂ treatment (Supplementary Table S3). Cyclin, calmodulin-related protein, calcium-transporting ATPase and transaldolase were all up-regulated.

Table 4 List of carbohydrate metabolism-related differentially expressed genes of *H. pluvialis* under two CO₂ concentrations

Gene ID	Log ₂ FC	Gene annotation
Unigene14387_All	7.44	Glucose-6-phosphate isomerase
Unigene22448_All	3.66	Glyceraldehyde 3-phosphate dehydrogenase
CL6807.Contig1_All	1.88	Phosphoglycerate kinase
CL10817.Contig1_All	4.08	Pyruvate kinase
Unigene3795_All	2.75	Pyruvate kinase
Unigene19963_All	- 2.27	Pyruvate kinase
Unigene31645_All	- 2.36	Pyruvate kinase
CL2951.Contig1_All	2.10	Mitochondrial aconitate hydratase
CL2951.Contig2_All	2.22	Mitochondrial aconitate hydratase
CL2951.Contig3_All	2.07	Mitochondrial aconitate hydratase
CL8074.Contig1_All	3.62	Isocitrate dehydrogenase, NAD-dependent
CL8074.Contig2_All	3.61	Isocitrate dehydrogenase, NAD-dependent
CL3305.Contig2_All	-2.41	Isocitrate dehydrogenase, NADP-dependent
CL3305.Contig3_All	-2.58	Isocitrate dehydrogenase, NADP-dependent
CL7051.Contig7_All	1.71	Malate dehydrogenase
CL9961.Contig2_All	- 2.98	Malate dehydrogenase
CL6807.Contig1_All	1.88	Phosphoglycerate kinase
CL2177.Contig2_All	2.95	6-Phosphogluconate dehydrogenase, decarboxylating
CL8925.Contig2_All	8.66	Glucose-6-phosphate dehydrogenase (G6PDH)
CL8925.Contig3_All	3.59	Glucose-6-phosphate dehydrogenase (G6PDH)
CL8925.Contig4_All	3.31	Glucose-6-phosphate dehydrogenase (G6PDH)
CL3573.Contig2_All	1.95	Acetyl-coenzyme A synthetase
Unigene22292_All	- 1.66	Acetyl-CoA synthetase-like protein
CL2733.Contig2_All	2.78	Formate C-acetyltransferase
CL2733.Contig3_All	2.11	Formate C-acetyltransferase
CL140.Contig2_All	2.15	Pyruvate formate lyase activating enzyme
CL2766.Contig1_All	1.95	Pyruvate decarboxylase
CL2766.Contig3_All	2.01	Pyruvate decarboxylase
CL5609.Contig3_All	3.40	Bidirectional sugar transporter
Unigene20709_All	3.57	Bidirectional sugar transporter SWEET7
CL10303.Contig1_All	7.94	Classical arabinogalactan protein 9-like
CL1012.Contig3_All	- 3.91	Classical arabinogalactan protein 4
CL2217.Contig1_All	- 3.07	Malate synthase mRNA
CL9309.Contig2_All	- 2.22	Sulfated surface glycoprotein185
Unigene20978_All	- 4.86	Sulfated surface glycoprotein185
CL5904.Contig3_All	- 2.01	Sulfated surface glycoprotein185
Unigene23043_All	- 3.56	Cellulose synthase
CL7979.Contig1_All	- 2.02	Cellulase
CL7668.Contig1_All	- 3.01	Starch synthase
CL7447.Contig1_All	- 3.92	Glycosyl hydrolases family 32 n
CL7742.Contig1_All	- 2.11	Exostosin-like glycosyltransferase
CL6205.Contig1_All	- 2.69	Glycosyl transferase group1 mRNA
CL8843.Contig4_All	- 1.77	Sedoheptulose-1,7-biphosphatase
Unigene15274_All	- 3.72	Beta-fructofuranosidase, insoluble isoenzyme CWINV3
Unigene15781_All	- 5.58	Acid beta-fructofuranosidase
Unigene32600_All	- 7.38	Carbohydrate-binding protein, putative
CL2345.Contig5_All	- 2.24	Glyoxal or galactose oxidase
Unigene13479_All	- 3.84	Phosphoglucan, water dikinase, chloroplastic

FC, fold changes of the gene expression (group 0.04% CO₂ vs. 0.16% CO₂)

In contrast, cell division protease FtsH, homogentisate phytyltransferase, and ornithine decarboxylase were all down-regulated. Several glutathione peroxidases and ubiquitin-protein ligases were also down-regulated.

GO and KEGG Enrichment Analysis of the DEGs

The 1665 DEGs were significantly enriched for 37 GO items (Supplementary Fig. S1). The "cellular process" (246 DEGs) and "metabolic process" (243 DEGs) terms were the two main functions enriched in the biological process category. In the cellular component category, the terms "cell" and "cell part" were the most highly enriched, accounting for 43.32% of the total enrichment in this category, followed by "organelles" (138 DEGs) and "membranes" (122 DEGs). In the molecular function category, "catalytic activity" (236 DEGs) and "binding" (202 DEGs) were the main functions enriched.

Of these DEGs, the significantly enriched KEGG pathways with the greatest numbers of DEGs were "Metabolic pathways" and "Genetic information processing" (Supplementary Fig. S2). Among the 20 KEGG subclasses, the largest number of DEGs were enriched in "Global and overview maps" (222 DEGs), followed by "Translation" (105 DEGs), "Folding, sorting and degradation" (102 DEGs), "Carbohydrate metabolism" (74 DEGs), "Transport and catabolism" (73 DEGs), "Transcription" (66 DEGs), and "Transport and catabolism" (73 DEGs).

Results of qPCR Validation

Of the 8 candidate DEGs screened by RNA-seq, 5 were up-regulated and 3 were down-regulated. The expression profiles of the 5 up-regulated unigenes from RNA-seq and qPCR analysis were essentially consistent, with differences only in fold changes (Supplementary Table S4). Among the 3 down-regulated unigenes, the fold change in the heat shock protein Hsp70C was identical between the HiSeq 2000 and qPCR results; however, ornithine decarboxylase 1 and malate dehydrogenase showed no significant decreases between the two groups by qPCR analysis. In conclusion, approximately 75% of the results were consistent with the HiSeq 2000 results, with differences only in fold changes, and 25% of the results showed no significant difference while the HiSeq 2000 results did. No opposite results were observed between the two methods.

PCA and OPLS-DA Analysis

A total of 693 peaks were extracted from the 12 samples, and 530 metabolites were retained after pretreatment. As shown from the PCA model (Fig. 4), the twelve samples

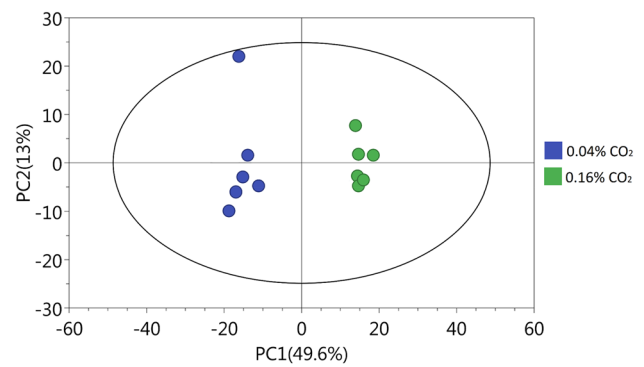


Fig. 4 Score scatter plot of PCA model for group 0.04% CO₂ versus 0.16% CO₂ of *H. pluvialis*. PC1, the first PCA component; PC2, the second PCA component. The integration value of the principal components is concentrated in Hotelling's T-squared ellipse

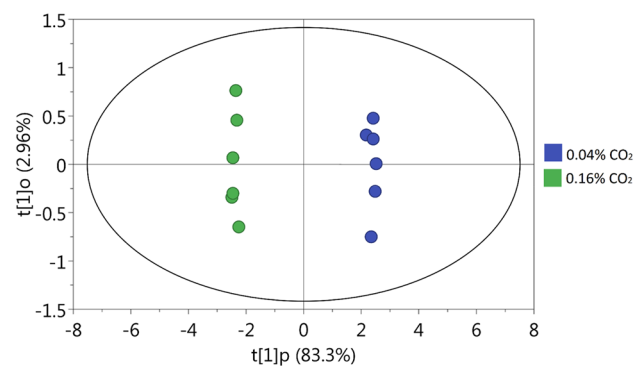


Fig. 5 Score scatter plot of OPLS-DA model for group 0.04% CO₂ versus 0.16% CO₂ of *H. pluvialis*. t[1]p, the predicted score of the first principal component; t[1]o, the orthogonal principal component score. The score scatter plot indicates the complete separation of the two groups, which suggests significant difference under two CO₂ concentrations

were significantly distinguished and located in 95% Hotelling's T-squared ellipse.

The quality of OPLS-DA model was tested by sevenfold cross validation (Fig. 5), and results showed that $R^2Y=0.998$ and $Q^2=0.992$, which can be deduced that the interpretability and predictability of the model is excellent. Permutation test showed that the intercept of $R^2=(0, 0.576)$ and $Q^2=(0, -0.46)$ (Supplementary Fig. S3), which proved that the model did not exist overfitting phenomenon.

Annotation of the Differential Metabolites

A total of 36 differential metabolites were identified from 0.16% CO₂ group compared to 0.04% CO₂ group (Table 5 and Fig. 3), and the hierarchical clustering analysis of the metabolites were shown in Fig. 6. Of the 36 metabolites, 5 metabolites including citric acid, ribose,

Table 5 List of differential metabolites of *H. pluvialis* under two CO₂ concentrations

Metabolites	Variable importance in the projection (VIP)	<i>p</i> value	Log ₂ FC
Citric acid	12.91	6.17E–09	4.73
Ribose	2.33	0.008559	4.19
3-Hydroxyanthranilic acid	1.69	0.000202	1.89
Glucose-1-phosphate	1.14	8.99E–07	1.16
1,3-Diaminopropane	2.07	0.020738	0.48
Ornithine ^a	1.80	1.47E–06	– 23.00
Aspartic acid ^a	1.42	3.05E–08	– 5.56
Tyrosine ^a	2.19	9.87E–10	– 3.65
Isoleucine	2.45	4.49E–11	– 3.46
4-Aminobutyric acid ^a	3.20	0.000211	– 3.42
Phenylalanine ^a	2.21	7.67E–10	– 3.27
Putrescine ^b	1.06	3.88E–06	– 3.16
Methionine ^a	1.40	2.86E–10	– 3.15
Valine	2.94	9.61E–12	– 3.11
Glycine ^a	1.51	1.54E–05	– 2.73
Galactose ^a	2.47	9.33E–08	– 2.65
Galactose ^b	1.22	1.07E–06	– 2.36
Phytol	6.00	4.29E–09	– 2.30
L-allothreonine ^a	1.71	1.60E–11	– 2.23
Glutamic acid	1.34	1.28E–09	– 2.19
Myo-inositol	1.67	8.73E–08	– 2.18
Proline	2.78	5.48E–08	– 2.18
L-malic acid	5.07	5.62E–06	– 2.17
Lysine	1.42	8.44E–07	– 2.05
Uracil	1.06	3.76E–07	– 1.81
Linolenic acid	2.10	0.000493	– 1.76
Oxoproline	6.37	1.74E–10	– 1.68
Threonic acid	4.87	1.95E–08	– 1.56
Glycine ^b	1.83	9.43E–05	– 1.55
Methyl-beta-D-galactopyranoside	3.13	2.16E–08	– 1.42
Alanine ^a	6.58	9.56E–08	– 1.38
Serine ^a	2.16	2.09E–07	– 1.36
Phosphate	3.02	1.05E–07	– 0.72
succinic acid	4.53	9.25E–05	– 0.70
Palmitic acid	1.45	0.007962	– 0.63
Ethanolamine	1.84	0.024906	– 0.54

FC, fold changes of the metabolites (group 0.04% CO₂ vs. 0.16% CO₂)

Different superscript letters represent the different derivatives of the same metabolites according to retention index

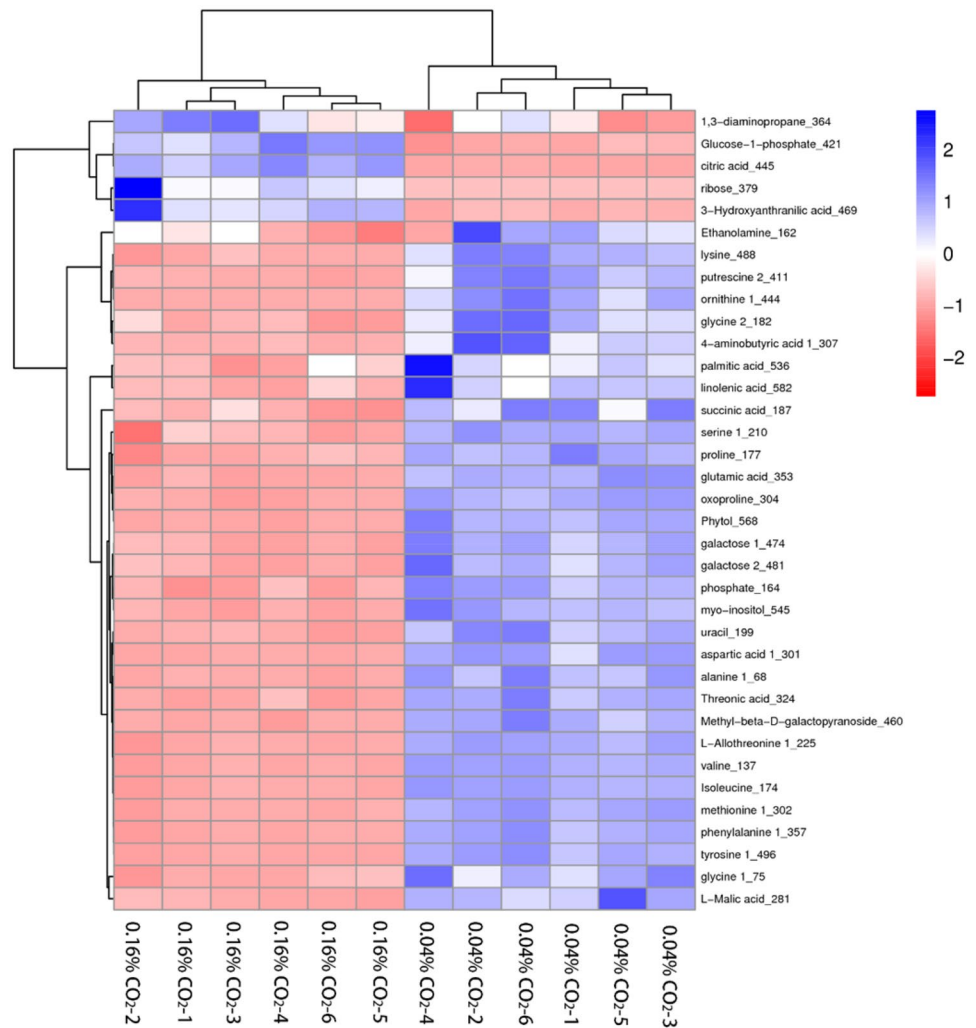
3-hydroxyanthranilic acid, glucose-1-phosphate, and 1,3-diaminopropane were increased; the content of citric acid and ribose in 0.16% CO₂ group was 26.50 and 18.32 times higher than that of the control group, respectively. Meanwhile, 31 metabolites contents decreased, including 14 amino acids, 2 fatty acids, 2 saccharide molecules, and 3 organic acid molecules. Of the 31 down-regulated metabolites, ornithine was the most significant, with a 2²³ times higher in the control group than that in 0.16% CO₂ group;

other amino acids such as aspartic acid, tyrosine, isoleucine, and phenylalanine were all abundant in 0.04% CO₂ group, with 47.18, 12.55, 11.00, and 9.65 times of that in 0.16% CO₂ group, respectively.

Pathway Analysis of the Differential Metabolites

Thirty-six metabolites were mapped into 55 KEGG pathways (Supplementary Table S5). Of them, the most

Fig. 6 Heatmap of hierarchical clustering analysis for differentially expressed metabolites of *H. pluvialis* under two CO₂ concentrations. Different color represents the relative quantity of the metabolites, with blue (up-regulation) and red (down-regulation)



differential pathway was “Metabolic pathways” (16), including citric acid, 4-aminobutyric acid, L-allothreonine, L-malic acid; next, the pathway of “Biosynthesis of plant secondary metabolites” and “Microbial metabolism in diverse environments”, each with 10 metabolites; the third, “Biosynthesis of secondary metabolites” and “Biosynthesis of antibiotics” possessed 9 metabolites.

The enrichment and topological analysis of the pathways of 36 metabolites were also performed (Supplementary Table S6), and the result is shown in a bubble diagram (Fig. 7). Each bubble represents a metabolic pathway and the most prominent enrichment pathway by enrichment analysis was “Biosynthesis of plant secondary metabolites” (18), with a *p* value of 1.15E−05 and an impact of 0.27; the biggest impact by topology analysis was the “Metabolic pathways” (15), with a *p* value of 0.92 and an impact of 2.26. Moreover, other pathways had been significantly enriched, including “Carbon metabolism” (18), “Biosynthesis of amino acids” (16), “Biosynthesis of secondary metabolites” (27), “Glycine, serine and threonine metabolism” (10), and

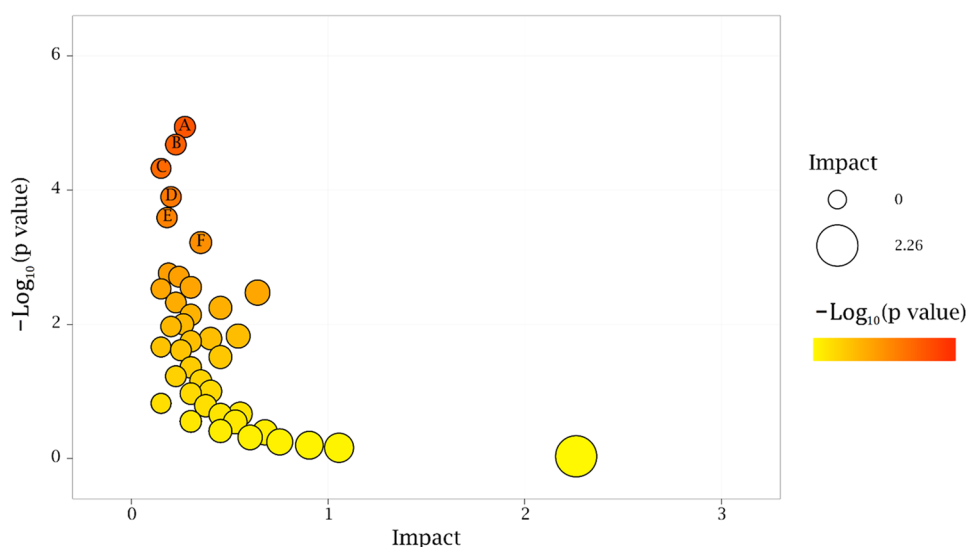
“Biosynthesis of alkaloids derived from ornithine, lysin and nicotinic acid” (6).

Discussion

Carbon source is one of the important components for astaxanthin production in *H. pluvialis*. Sodium acetate can significantly enhance the accumulation of astaxanthin (Zhang et al. 2018), but along with contamination and lower cell activity (Pang and Chen 2017). Photoautotrophic induction is effective in achieving high astaxanthin productivity with addition of bicarbonate or CO₂ (Kang et al. 2005). In this study, a relatively high CO₂ concentration was used to promote the growth of *H. pluvialis* at the vegetative stage, and the mechanism of this promotion was revealed through the analysis of transcriptome and metabolome.

Photosystem I, photosystem II, ATP synthase, and cytochrome b6/f complexes are the important components in the light reactions, photosynthetic phosphorylation and

Fig. 7 KEGG pathway enrichment analysis of *H. pluvialis* under two CO₂ concentrations. The size of the bubble indicates the influence factor of the topological analysis; the color indicates the significance of the enrichment analysis. **a:** Biosynthesis of plant secondary metabolites; **b** central carbon metabolism in cancer; **c** mineral absorption; **d** protein digestion and absorption; **e** cyanoamino acid metabolism; **f** aminoacyl-tRNA biosynthesis



electron transport (Yamori et al. 2011). In this study, the transcript expressions of the photosynthesis-related DEGs were all up-regulated in response to the increased CO₂ level. In addition, the mRNA abundances of diverse ribosomal proteins (12 DEGs), and cell division proteins (5DEGs) were also up-regulated by 0.16% CO₂ (Table 3). In summary, of the 46 photosynthesis- and chloroplast-related DEGs, 42 were promoted and only 4 were depressed by the elevated CO₂ level. Thus, the elevated CO₂ promoted the photosynthesis in *Haematococcus* cells, which is consistent with the change of photosynthesis efficiency at different CO₂ levels (Liu et al. 2016; Masle 2000).

Glycolysis is the initial enzymatic reaction of glucose catabolism, which can convert glucose into pyruvate. A series of enzymes including PGK, glucose-6-phosphate isomerase, and glyceraldehyde 3-phosphate dehydrogenase are participated in the glycolysis pathway. Of them, PGK is a major enzyme in the first ATP-generating step in this pathway. In this study, the mRNA levels of the three enzymes were all up-regulated by 0.16% CO₂. Two genes encoding pyruvate kinase responsible for the final step in glycolysis, were stimulated by the elevated CO₂ concentration. Similarly, 3.5-fold up-regulation of pyruvate kinase has been detected by 15% CO₂ in a mutant *H. pluvialis* (Cheng et al. 2017). Therefore, glycolysis was enhanced and large amounts of pyruvate and acetyl-CoA were synthesized from glycolysis pathway in 0.16% CO₂ group. More acetyl-CoA were flowed into TCA cycle than into lipid synthesis (the lipid content decrement in 0.16% CO₂ group). Citric acid is produced by the condensation of oxaloacetate and acetyl-CoA in TCA cycle, and its content was significantly enhanced at 0.16% CO₂ level, as shown in GC-MS results.

TCA cycle plays an important role in the energy metabolism, which is the link of carbohydrate, lipid, and amino acid metabolism. In the RNA-seq results, the encoding

genes of aconitase, isocitrate dehydrogenase, and malate dehydrogenase participated in TCA cycle were most up-regulated at 0.16% CO₂ level (Fig. 3 and Table 4). In the results of GC-MS, the contents of succinic acid and malic acid were reduced (Fig. 3 and Table 5). Therefore, it can be deduced that TCA cycle is enhanced by the up-regulation of the mitochondrial enzymes, coupled with the fast utilization of its intermediate metabolites at 0.16% CO₂ level. This result was different from the report that the level of TCA cycle decreased slightly at elevated [CO₂] in *Arabidopsis* (Liu et al. 2016), because CO₂ slows the daytime conversion of nitrate into protein, which reduces the activity of mitochondrial enzymes, such as succinate dehydrogenase and cytochrome c oxidase (Asensio et al. 2015). These results demonstrated that glycolysis and TCA cycle in *H. pluvialis* are promoted by the elevated CO₂ concentration.

Pentose phosphate pathway is another carbohydrate metabolic pathway in cells, which can catalyze glucose-1-phosphate into ribose-5-phosphate. In this study, the expression of two enzymes, 6-phosphogluconate dehydrogenase (decarboxylating) and G6PDH were all up-regulated, meanwhile, the related product of pentose phosphate pathway, ribose was accumulated in 0.16% CO₂ group (Tables 4 and 5). These results indicated that the pentose phosphate pathway was stimulated by 0.16% CO₂.

Nitrogen is the necessary nutritional component in plant growth and development. Many nitrogen-related genes, especially those of nitrate metabolism including nitrite reductase, nitrate reductase, and multiple nitrate transporters, were promoted in 0.16% CO₂ group. These results indicated that nitrogen metabolism was accelerated by the elevated CO₂ level (Supplementary Table S3). However, 12 kinds of common protein amino acids including valine, glycine, alanine, isoleucine, serine, proline, aspartic acid, methionine, glutamic acid, phenylalanine, lysine, and

tyrosine were all decreased under 0.16% CO₂ condition (Table 5). These amino acids might be used to the protein biosynthesis, which was confirmed by the increased levels of the soluble proteins in the 0.16% CO₂ group. The aforementioned results showed that assimilation of inorganic nitrogen, and protein synthesis were promoted by the elevated CO₂ level.

In contrast to the aforementioned metabolic pathways, which were promoted by the elevated CO₂ concentration, some stress-related substances and proteins was decreased. On the one hand, a total of 17 heat shock proteins and chaperones (only one exception), were decreased by 0.16% CO₂ (Supplementary Table S3). Heat shock proteins are referred to as stress proteins in organisms, which perform functions under the environmental conditions (Parsell and Lindquist 1993). On the other hand, the stress-related substrates such as ornithine, putrescine, proline, and 4-aminobutyric acid were all depressed by 0.16% CO₂. The non-protein amino acid ornithine can be produced from glutamic acid in plants, and putrescine can be synthesized by the decarboxylation of arginine or ornithine (Rio et al. 2018). Ornithine can accumulate a high level and increased the tolerance against the adverse conditions (Kalamaki et al. 2009). Putrescine, proline, and 4-aminobutyric acid all function in the abiotic stress tolerance (Durmu and Kadioğlu 2005; Kishor et al. 2005; Bouche et al. 2003). In the present study, these stress-related proteins, amino acid, and polyamine were all down-regulated under the elevated CO₂ condition, indicating that 0.16% CO₂ might be more conducive to the fast growth of *H. pluvialis* than 0.04% CO₂.

Conclusion

In the green vegetative stage of *H. pluvialis*, the elevated CO₂ concentration is beneficial for the algal growth. The enzymes, proteins, and metabolites involved in the photosynthesis, TCA cycle, glycolysis, nitrogen metabolism, and protein synthesis, were mainly promoted by the elevated CO₂ level in order to provide the material and energy for growth. Instead, heat shock proteins and resistance-related metabolites such as ornithine, proline, and putrescine were all decreased. Taken together, these resulted in the fast growth of *H. pluvialis* under 0.16% CO₂ condition.

Acknowledgements This work was supported by the National Natural Science Foundation of China (31572638). This research was also sponsored by the K. C. Wong Magna Fund in Ningbo University.

Author Contributions XY and JC were responsible of the laboratory work and manuscript preparation; CH contributed to data analysis and manuscript revision; NX and XS contributed to the experimental design and manuscript modification.

Data Availability The raw reads were deposited in the Short Read Archive (SRA) database (<https://www.ncbi.nlm.nih.gov/sra/>) under the accession number of SRR9008963-9008965 and SRR8893734-8893736.

Compliance with Ethical Standards

Conflict of interest The authors have no potential conflicts of interest to report.

References

- Abdi H, Williams LJ (2010) Principal component analysis. *Wiley Interdiscip Rev Comput Stat* 2:433–459
- Asensio JS, Rachmilevitch S, Bloom AJ (2015) Responses of *Arabidopsis* and wheat to rising CO₂ depend on nitrogen source and nighttime CO₂ levels. *Plant Physiol* 168:156–163
- Bouche N, Fait A, Bouchez D, Møller SG, Fromm H (2003) Mitochondrial succinic-semialdehyde dehydrogenase of the gamma-aminobutyrate shunt is required to restrict levels of reactive oxygen intermediates in plants. *PNatl Acad Sci USA* 100:6843–6848
- Boussiba S (2000) Carotenogenesis in the green alga *Haematococcus pluvialis*: cellular physiology and stress response. *Physiol Plantarum* 108:111–117
- Chang L, Sui Z, Fu F, Zhou W, Wang J, Kang K, Zhang S, Ma J (2014) Relationship between gene expression of UDP-glucose pyrophosphorylase and agar yield in *Gracilariaopsis lemaneiformis* (Rhodophyta). *J Appl Phycol* 26:2235–2441
- Cheng J, Li K, Zhu Y, Yang W, Zhou J, Cen K (2017) Transcriptome sequencing and metabolic pathways of astaxanthin accumulated in *Haematococcus pluvialis* mutant under 15% CO₂. *Bioresour Technol* 228:99–105
- Christian D, Zhang J, Sawdon AJ, Peng CA (2018) Enhanced astaxanthin accumulation in *Haematococcus pluvialis* using high carbon dioxide concentration and light illumination. *Bioresour Technol* 256:548–551
- Conesa A, Götz S, García-Gómez JM, Terol J, Talon M (2005) Blast2GO: a universal tool for annotation, visualization and analysis in functional genomics research. *Bioinformatics* 21:3674–3676
- Durmu N, Kadioğlu A (2005) Spermine and putrescine enhance oxidative stress tolerance in maize leaves. *Acta Physiol Plant* 27:515–522
- Gao Z, Li Y, Wu G, Li G, Sun H, Deng S, Shen Y, Chen G, Zhang R, Meng C, Zhang X (2015) Transcriptome analysis in *Haematococcus pluvialis*: astaxanthin induction by salicylic acid (SA) and jasmonic acid (JA). *PLoS ONE* 10:e0140609
- Hagen C, Siegmund S, Braune W (2002) Ultrastructural and chemical changes in the cell wall of *Haematococcus pluvialis* (Volvocales, Chlorophyta) during aplanospore formation. *Euro J Phycol* 37:217–226
- Huang JC, Chen F, Sandmann G (2006) Stress-related differential expression of multiple β -carotene ketolase genes in the unicellular green alga *Haematococcus pluvialis*. *J Biotechnol* 122:176–185
- Imamoglu E, Sukan FV, Dalay MC (2007) Effect of different culture media and light intensities on growth of *Haematococcus pluvialis*. *Int J Nat Eng Sci* 1:5–9
- Kalamaki MS, Alexandrou D, Lazari D, Merkouropoulos G, Fotopoulos V, Pateraki I, Aggelis A, Carrillo-López A, Rubio-Cabetas MJ, Kanellis AK (2009) Over-expression of a tomato N-acetyl-L-glutamate synthase gene (SINAGS1) in *Arabidopsis thaliana* results in high ornithine levels and increased tolerance in salt and drought stresses. *J Exp Bot* 60:1859–1871

- Kanehisa M, Sato Y, Kawashima M, Furumichi M, Tanabe M (2015) KEGG as a reference resource for gene and protein annotation. *Nucleic Acids Res* 44:D457–462
- Kang CD, Lee JS, Park TH, Sim SJ (2005) Comparison of heterotrophic and photoautotrophic induction on astaxanthin production by *Haematococcus pluvialis*. *Appl Microbiol Biotechnol* 68:237–241
- Kishor PBK, Sangam S, Amrutha RN (2005) Regulation of proline biosynthesis, degradation, uptake and transport in higher plants: its implications in plant growth and abiotic stress tolerance. *Curr Sci* 54:271–275
- Kushihiro H, Minakuchi F, Fukui I (1972) Evaluation of the determination method for serum total lipids. 2. Colorimetric method by sulfo-phospho-vanillin reaction. *Rinsho Byori* 20:135–138
- Langmead B, Salzberg SL (2012) Fast gapped-read alignment with Bowtie 2. *Nat. Methods* 9:357–359
- Lee C, Ahn JW, Kim JB, Kim JY, Choi YE (2018) Comparative transcriptome analysis of *Haematococcus pluvialis* on astaxanthin biosynthesis in response to irradiation with red or blue LED wavelength. *World J Microbiol Biotechnol* 34:96–109
- Li B, Dewey CN (2011) RSEM: accurate transcript quantification from RNA-Seq data with or without a reference genome. *BMC Bioinformatics* 12:323–338
- Liu L, Shen F, Xin C, Wang Z (2016) Multi-scale modeling of *Arabidopsis thaliana* response to different CO₂ conditions: from gene expression to metabolic flux. *J Integr Plant Biol* 58:2–11
- Livak KJ, Schmittgen TD (2001) Analysis of relative gene expression data using real-time quantitative PCR and the 2^{-ΔΔCT} method. *Methods* 25:402–408
- Lv H, Xia F, Liu M, Cui X, Wahid F, Jia S (2016) Metabolomic profiling of the astaxanthin accumulation process induced by high light in *Haematococcus pluvialis*. *Algal Res* 20:35–43
- Mackinney G (1941) Absorption of light by chlorophyll solution. *J Biol Chem* 140:315–322
- Morris DL (1948) Quantitative determination of carbohydrates with dreywood's anthrone reagent. *Science* 107:254–255
- Pang N, Chen S (2017) Effects of C5 organic carbon and light on growth and cell activity of *Haematococcus pluvialis* under mixotrophic conditions. *Algal Res* 21:227–235
- Parsell D, Lindquist S (1993) The function of heat-shock proteins in stress tolerance: degradation and reactivation of damaged proteins. *Annu Rev Genet* 27:437–496
- Quevillon E, Silventoinen V, Pillai S, Harte N, Mulder N, Apweiler R, Lopez R (2005) InterProScan: protein domains identifier. *Nucleic Acids Res* 33:W116–120
- Rio BD, Alvarez-Sieiro P, Redruello B, Martin MC, Fernandez M, Ladero V, Alvarez M (2018) *Lactobacillus rossiae* strain isolated from sourdough produces putrescine from arginine. *Sci Rep* 8:3989–3998
- Su Y, Wang J, Shi M, Niu X, Yu X, Gao L, Zhang X, Chen L, Zhang W (2014) Metabolomic and network analysis of astaxanthin-producing *Haematococcus pluvialis* under various stress conditions. *Bioresour Technol* 170:522–529
- Tarazona S, Garcia-Alcalde F, Dopazo J, Ferrer A, Conesa A (2011) Differential expression in RNA-seq: a matter of depth. *Genome Res* 21:2213–2223
- Tsugawa H, Tsujimoto Y, Arita M, Bamba T, Fukusaki E (2011) GC/MS based metabolomics: development of a data mining system for metabolite identification by using soft independent modeling of class analogy (SIMCA). *BMC Bioinformatics* 12:131–143
- Walker J (1994) The bicinchoninic acid (BCA) assay for protein quantitation. *Methods Mol Biol* 32:5–8
- Wan M, Zhang J, Hou D, Fan J, Li Y, Huang J, Wang J (2014) The effect of temperature on cell growth and astaxanthin accumulation of *Haematococcus pluvialis* during a light-dark cyclic cultivation. *Bioresour Technol* 167:276–283
- Wang J, Zhou C, Yan X, Luo Q, Jiang Y, Ma B, Tan Y (2014) The characteristics of growth and nutrient consumption of *Haematococcus pluvialis* under red light. *Acta Hydrobiol Sinica* 38:1135–1142 (in Chinese)
- Wayama M, Ota S, Matsuura H, Nango N, Hirata A, Kawano S (2013) Three-dimensional ultrastructural study of oil and astaxanthin accumulation during encystment in the green alga *Haematococcus pluvialis*. *PLoS ONE* 8:e53618
- Wiklund S, Johansson E, Sjoestrom L, Mellerowicz EJ, Edlund U, Shockcor JP, Gottfries J, Moritz T, Trygg J (2008) Visualization of GC/TOF-MS-based metabolomics data for identification of biochemically interesting compounds using OPLS class models. *Anal Chem* 80:115–122
- Yamori W, Takahashi S, Makino A, Price GD, Badger MR, von Caemmerer S (2011) The roles of atp synthase and the cytochrome b6/f complexes in limiting chloroplast electron transport and determining photosynthetic capacity. *Plant Physiol* 155:956–962
- Zhang C, Zhang L, Liu J (2018) Exogenous sodium acetate enhances astaxanthin accumulation and photoprotection in *Haematococcus pluvialis* at the non-motile stage. *J Appl Phycol* 30:1–8

Publisher's Note Springer Nature remains neutral with regard to jurisdictional claims in published maps and institutional affiliations.